

Nanosphere Lithography: Effect of Substrate on the Localized Surface Plasmon Resonance Spectrum of Silver Nanoparticles

Michelle Duval Malinsky, K. Lance Kelly, George C. Schatz,^{*,†} and Richard P. Van Duyne^{*,‡}

Department of Chemistry, Northwestern University, Evanston, Illinois 60208-3113

Received: August 11, 2000; In Final Form: December 8, 2000

In this paper, we explore the optical contributions of the substrate to the localized surface plasmon resonance (LSPR) spectrum of surface confined Ag nanoparticles produced by nanosphere lithography (NSL). We present optical extinction spectra of Ag nanoparticles fabricated on the following substrates: fused silica, borosilicate optical glass, mica, and SF-10—a high refractive index specialty glass. For all the experiments discussed here, the Ag nanoparticles were approximately 100 nm in in-plane width and 25 nm in out-of-plane height. In a controlled N₂ environment, the wavelength corresponding to the extinction maximum, λ_{max} , shifts to the red with increasing refractive index of the substrate, $n_{\text{substrate}}$. The sensitivity factor, $\Delta\lambda_{\text{max}}/\Delta n_{\text{substrate}}$, was measured to be 87 nm per refractive index unit (RIU). Experimental extinction spectra were modeled using the discrete dipole approximation (DDA). The DDA theory qualitatively predicts the experimentally observed trend that λ_{max} is linearly dependent on $n_{\text{substrate}}$; however, the theory overestimates the sensitivity by approximately a factor of 2. The sensitivity of the LSPR to the refractive index of bulk external solvent, n_{external} , was also examined for each of the four substrates listed above. For all the cases, the change in λ_{max} in response to bulk external solvent was linearly dependent upon n_{external} . Values of the sensitivity factors, $\Delta\lambda_{\text{max}}/\Delta n_{\text{external}}$, ranged from 206 nm RIU⁻¹ for mica to 258 nm RIU⁻¹ for SF-10, a difference of only 25%. From the results presented here, we conclude that there is no systematic dependence, or at most a weak dependence, which correlates the bulk solvent sensitivity of the LSPR to $n_{\text{substrate}}$. The DDA theory overestimates the LSPR sensitivity to bulk external environment, but the ratio of solvent to substrate sensitivity factors is correct within experimental uncertainty. This ratio has a value of approximately 2, which indicates that there is greater sensitivity in the optical response to the solvent than to the substrate. This ratio is within 10% of the ratio of areas of the particles that are exposed to solvent and substrate. We suggest that chemical interactions at the interfaces between the nanoparticle and the substrate and/or the nanoparticle and the bulk environment contribute significantly to the observed difference between experimental and theoretical sensitivity factors.

I. Introduction

When noble metal nanoparticles are excited by electromagnetic radiation, they exhibit collective oscillations of their conduction electrons that result in both absorption and scattering of the incident radiation.¹ The extinction spectrum, which is the sum of the absorption and scattering spectra, of such nanoparticles in a vacuum, solution, or supported on the surface of a substrate is often measured in transmission geometry using a UV–vis spectrophotometer. In a simple situation, such as that of nearly monodisperse spherical gold nanoparticles in solution, the extinction spectrum exhibits a single peak known as the localized surface plasmon resonance (LSPR). In addition to wavelength-selective photon absorption and scattering, an important consequence of LSPR excitation is the local electromagnetic field enhancement that lies at the heart of surface-enhanced spectroscopy.²

The wavelength corresponding to the extinction maximum, λ_{max} , of the LSPR is highly dependent on the size, shape, interparticle spacing, and wavelength-dependent dielectric constants of the material from which the nanoparticles are composed. In addition, the λ_{max} of the LSPR is dependent on the dielectric properties of (1) the local environment that surrounds

the nanoparticles and (2) the substrate, if any, on which the particles are supported.^{1,3} The ability to manipulate and predict the LSPR of metal nanoparticle systems is desirable in several technological applications including, but not limited to the following: optical devices,^{4,5} optical energy transport,^{6–9} near field scanning optical microscopy (NSOM),^{10–14} surface-enhanced spectroscopies,^{15–23} and chemical and biological sensors.^{24–27}

Nanosphere lithography (NSL) is a powerful fabrication technique for the creation of arrays of nanoparticles with controlled size, shape, and interparticle spacing.^{28,29} Briefly, a two-dimensional (2D) colloidal crystal deposition mask is self-assembled from size-monodisperse nanospheres of diameter, D , forming a hexagonally close-packed monolayer on a substrate. A metal or other material is then deposited by thermal evaporation, electron-beam deposition, or pulsed laser deposition through the mask to a controlled mass thickness, d_m . After deposition, the nanosphere mask is removed by sonicating the entire sample in a solvent. An array of triangularly shaped particles with P_{6mm} symmetry remains on the substrate. The in-plane width a and out-of-plane height b of NSL-fabricated nanoparticles can be independently tuned with few nanometer precision by manipulation of the parameters D and d_m . Nanoparticle shape is controlled by the precision of the 2D colloidal crystal mask or, alternatively, by postdeposition processing steps

* To whom correspondence should be addressed.

† E-mail: schatz@chem.nwu.edu.

‡ E-mail: vanduyne@chem.nwu.edu.

such as thermal annealing. Additionally, NSL is quite simple, inexpensive, and materials-general, which makes it nearly ideal as a platform for theory vs experiment studies of nanoparticle optical properties.^{30,31} Recently, we have used NSL to establish that the extinction maximum, λ_{\max} , of the LSPR of Ag nanoparticles can be tuned throughout the visible and infrared regions by independently and systematically varying the in-plane width, out-of-plane height, and dielectric environment of the nanoparticles.^{31,32} From these detailed investigations of the size-, shape-, and dielectric-dependent optical properties of Ag nanoparticles, we have created a new class of nanosensors.³³ With these sensors, measured shifts of λ_{\max} are used to detect changes in local dielectric environment induced by analyte binding events to NSL-fabricated Ag nanoparticles chemically modified with functionalized self-assembled monolayers (SAMs).

As mentioned above, the implementation of nanoparticles into device applications is one of the underlying motivations for the study of nanoparticle optics. Realization of this objective will most likely involve isolating or embedding nanoparticle constituents on or in a solid substrate support. Thus, determining the substrate contribution to the optical properties of the supported nanoparticles is an important endeavor. The influence of the substrate on the LSPR of small (~ 2 nm diameter) Ag nanoparticles formed in a cluster beam with various seeding gases and deposited on various substrates under ultrahigh vacuum conditions has been previously studied.^{3,27} A 50 nm red shift in the λ_{\max} of the LSPR was observed by comparing free Ag nanoparticles in a vacuum with those supported on SiO₂. In this situation, the position of the Mie or localized surface plasmon resonance (LSPR) is determined by the following factors: (1) the dielectric properties of the substrate and surrounding medium; (2) the nanoparticle size-dependent dielectric constants of Ag; (3) cluster shape deformation caused by collision with and/or wetting by the substrate; and (4) static and dynamic charge transfer at the cluster/substrate interface. Compelling evidence is given indicating that cluster shape deformation as well as static and dynamic charge-transfer effects are significant in determining the influence of the substrate on the LSPR extinction maximum. In the work presented here, we examine how the LSPR of large (~ 100 nm in-plane by ~ 25 nm out-of-plane) Ag nanoparticles is influenced by the refractive index of the substrate, $n_{\text{substrate}}$. In this circumstance, nanoparticle structure is reasonably well-defined from atomic force microscopy (AFM) measurements, the dielectric constant of the Ag should be very close to that of bulk Ag, and the role of static and dynamic charge transfer at the cluster/substrate interface should be minimized since the number of surface atoms is a small fraction of the total number of atoms. To the best of our knowledge, no prior theory vs experiment studies of the substrate effect for nanoparticles in this size regime exist.

We will present UV-vis extinction spectra of Ag nanoparticles in a controlled N₂ environment on each of the following substrates: fused silica, borosilicate optical glass, mica, and SF-10—a specialty glass with high refractive index. An implementation of electrodynamic theory known as the discrete dipole approximation (DDA) is used to model the experimentally measured extinction spectra. The sensitivity of λ_{\max} to bulk external solvent is also examined for each of the substrates. We demonstrate the following: (1) λ_{\max} of the LSPR is dependent upon the optical properties of the supporting substrate with a sensitivity factor, $\Delta\lambda_{\max}/\Delta n_{\text{substrate}}$, of 87 nm per refractive index unit (RIU); (2) DDA accurately predicts this observed trend, but produces a value of $\Delta\lambda_{\max}/\Delta n_{\text{substrate}}$ of 155 nm RIU⁻¹, almost twice that measured experimentally; (3) the sensitivity

factor of the LSPR to bulk dielectric environment, $\Delta\lambda_{\max}/\Delta n_{\text{external}}$, ranges from 206 nm RIU⁻¹ for mica to 258 nm RIU⁻¹ for SF-10, a difference of 25%; and (4) theory overestimates the solvent effect, but the DDA ratio of solvent and substrate sensitivities is accurate. We will also study the correlation of this ratio to the exposed areas of nanoparticles that are in contact with solvent and substrate, and we will examine solvent shifts for solvents that are indexed matched to the substrate.

The remainder of this paper will proceed as follows. In section II, we discuss the experimental and theoretical details used to fabricate, characterize, and model the Ag nanoparticles presented here. In section III, we present and discuss our experimental results and compare them to theoretical calculations when appropriate. Section IV summarizes our results and conclusions.

II. Experimental Section

A. Materials. Ag (99.99%, 0.50 mm diameter) was purchased from D. F. Goldsmith (Evanston, IL). Ruby red muscovite mica was purchased from Asheville-Schoonmaker (Newport News, VA) in the form of 50 mm sheets. Borosilicate glass substrates were No. 2 coverslips acquired from Fisher Scientific (Fairlawn, NJ). Fused silica and SF-10 substrates were purchased from Esco Products (Oak Ridge, NJ) and Schott Glass Technologies (Duryea, PA), respectively. Polystyrene nanospheres ($D = 400 \pm 7$ nm) were acquired from Interfacial Dynamics Corporation (Portland, OR) and were used as received. Tungsten vapor deposition boats were obtained from R. D. Mathis Corporation (Long Beach, CA). The following solvents and chemicals were used as received from their respective vendors: methanol, acetone, methylene chloride, benzene, H₂SO₄, H₂O₂, NH₄OH, all from Fisher Scientific; ethanol, from Pharmco (Brookfield, CT); and carbon tetrachloride, from Aldrich (Milwaukee, WI). Nitrogen gas used for drying and controlling the nanoparticle environment was purchased from Air Products (Allentown, PA) and passed through a particulate filter and a tube packed with Drierite from W. A. Hammond Drierite Co. (Xenia, OH). For all steps of substrate preparation, water purified with cartridges from Millipore (Marlborough, MA) to a resistivity of 18 M Ω was used.

B. Substrate Preparation. Borosilicate glass, fused silica, and SF-10 substrates were cleaned by immersion in piranha solution (3:1 concentrated H₂SO₄:30% H₂O₂) at 80 °C for 1 h. After cooling, the substrates were rinsed repeatedly with Millipore water and then sonicated for 60 min in 5:1:1 H₂O:NH₄OH:30% H₂O₂ solution. Following sonication, the substrates were again rinsed repeatedly with water and then used immediately or stored in water for no longer than 1 week. Mica substrates were either used as received or freshly cleaved immediately before nanosphere mask formation. All substrates were circular in shape with 18 mm diameters so as to function as windows in a UV-vis extinction flow cell described elsewhere.³³

C. Nanoparticle Preparation. Single-layer periodic particle arrays were prepared using the technique of nanosphere lithography.^{28,29} To form the deposition mask, approximately 2–3 μL of the nanosphere solution was drop coated onto the 18 mm substrates. Once the 2D colloidal crystal deposition mask was formed, the substrates were mounted into the chamber of a Consolidated Vacuum Corporation vapor deposition system. Ag films of various thicknesses were then deposited over the nanosphere mask. The mass thickness, d_m , for each film was measured using a Leybold Inficon XTM/2 deposition monitor quartz crystal microbalance (East Syracuse, NY). After the Ag deposition, the nanosphere mask was removed by sonicating the entire substrate in absolute ethanol for 2 min.

D. Atomic Force Microscopy (AFM) Measurements. AFM images were collected under ambient conditions using either a Digital Instruments Nanoscope III or Digital Instruments Bioscope operating in either contact mode or tapping mode. Etched Si nanoprobe tips (Digital Instruments, Santa Barbara, CA) with spring constants of approximately 0.15 N m^{-1} were used. These conical-shaped tips had a cone angle of 20° and an effective radius of curvature of 10 nm. The resonance frequency of the tapping mode cantilevers was measured to be between 280 and 330 kHz. The AFM images presented here represent raw, unfiltered data.

E. Ultraviolet–Visible Extinction Spectroscopy. UV–vis extinction measurements were performed on an Ocean Optics (Dunedin, FL) SD2000 fiber optically coupled spectrophotometer with a CCD detector. All spectra shown here were macroscopic measurements performed in transmission geometry using unpolarized light at normal incidence with a probe beam size of approximately 5 mm^2 . Each spectrum is the average of 25 individual 100 ms integrations. In a previous study, we demonstrated that macroextinction spectra with probe beam areas of 4 mm^2 or greater are equivalent to spatially resolved microextinction spectra with probe beam areas of $12 \mu\text{m}^2$.³¹ Thus, Ag island defect sites caused by imperfections in the nanosphere mask do not contribute appreciably to the LSPR. Samples were placed in a custom-built flow cell so that the nanoparticle environment could be controlled at all times.³³ Prior to recording any spectra, various solvents (methanol, acetone, ethanol, and methylene chloride) followed by dry N_2 gas were cycled through the flow cell until the extinction spectrum of the nanoparticles repeatedly returned to the same spectral location in N_2 . In a recent study, we demonstrated that when exposed to various solvents—such as methanol, acetone, and water—NSL-fabricated Ag nanoparticles undergo slight changes in shape and height. These small changes in structural morphology can have quite significant effects on the optical properties shifting λ_{max} by over 100 nm.³³ Thus, the solvent cycling described above was performed to force the nanoparticles into their most stable structural state prior to determining the sensitivity to bulk external solvent.

F. Discrete Dipole Approximation. The DDA is a numerical solution of Maxwell's equations which can generate the absorption, scattering, and extinction cross sections nearly exactly for particles of arbitrary shape. The full details of this method have been described elsewhere.^{30,34–36} Briefly, DDA involves replacing the particle of interest with an array of cubic dipoles. The polarizability of each element is assigned based on bulk dielectric constants, with the constraint that the optical response of a bulk lattice of dipoles match that obtained using continuum electrodynamics. The dipole polarizations are then solved self-consistently for an incident plane wave field. The strength of this method lies in its ability to directly calculate the optical response of a nanoparticle without any fitting parameters given that the following aspects are known: (1) nanoparticle size and shape, (2) bulk dielectric constants of each material (size-dependent effects should be small for particles as large as we are studying), and (3) incident wavelengths. Furthermore, DDA can be used to model systems composed of more than one material, as is done here. For the calculations presented in this study, the NSL-fabricated Ag nanoparticle is represented by a truncated tetrahedron³⁰ and the substrate is approximated to be a flat cylindrical slab. Calculations were performed using the publicly available program DDSCAT version 5a9 by Draine and Flatau.³⁷ The wavelength-dependent dielectric constants for Ag were obtained from Palik.³⁸

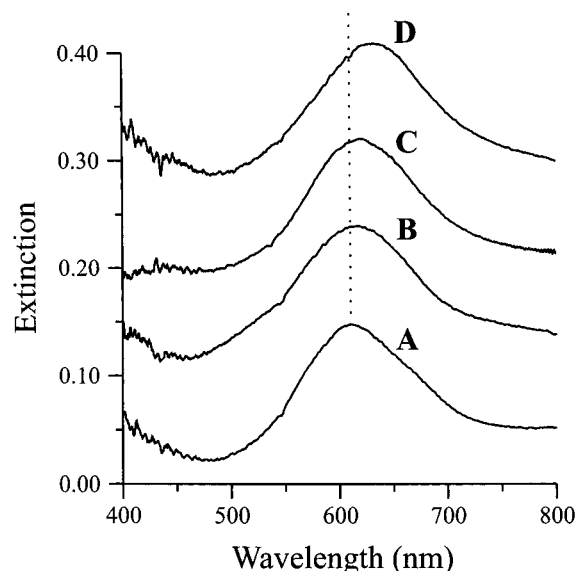


Figure 1. UV–vis extinction spectra of Ag nanoparticles on various substrates in a N_2 environment. All nanoparticles were fabricated using $D = 400 \text{ nm}$ nanospheres and $d_m = 25 \text{ nm}$. The spectra have been arbitrarily spaced along the extinction axis for clarity. (A) Fused silica ($n = 1.46$); $\lambda_{\text{max}} = 611 \text{ nm}$. (B) Borosilicate optical glass ($n = 1.52$); $\lambda_{\text{max}} = 616 \text{ nm}$. (C) Mica ($n = 1.6$); $\lambda_{\text{max}} = 622 \text{ nm}$. (D) SF-10 ($n = 1.73$); $\lambda_{\text{max}} = 635 \text{ nm}$.

III. Results and Discussion

A. Substrate Effects for Ag Nanoparticles in N_2 or a Vacuum. Previously, we demonstrated that the LSPR λ_{max} of Ag nanoparticles prepared using NSL depends on the external dielectric properties of the nanoparticles' environment.³¹ For these studies, the external nanoparticle environment consisted of (1) the mica substrates on which the nanoparticles were fabricated and (2) the solvent or gas that surrounded the entire sample. The work presented here continues the examination of the external dielectric dependent optical properties of Ag nanoparticles. In this section, the surrounding bulk environment is restricted to N_2 ($n_{\text{external}} = 1.0$) while the refractive index of the substrate ($n_{\text{substrate}}$) is varied from 1.46 to 1.73. Figure 1 displays a collection of extinction spectra for solvent-treated Ag nanoparticles fabricated with aspect ratio = 4:1 (width: height) on the following substrates: fused silica ($n = 1.46$), borosilicate glass ($n = 1.52$), mica ($n = 1.6$), and SF-10 ($n = 1.73$). Because some sample to sample variation occurs, the spectra shown in Figure 1 are all representative examples observed during several experiments. In Figure 1, λ_{max} systematically shifts to the red from 611 nm for nanoparticles on fused silica, the substrate with the lowest refractive index, to 634 nm for nanoparticles on SF-10, the substrate with the highest refractive index. Figure 2 shows AFM images of the Ag nanoparticles on the various substrates used to generate the extinction spectra in Figure 1. From the AFM images, it appears that nanoparticle shapes are independent of substrate. Slight differences in the images can be attributed to variation in AFM probe tip quality. Thus, the Ag nanoparticles are prone to the same level of solvent-induced morphology changes despite differences in the chemical composition of the substrate to which they are confined. Therefore, the shifts in the LSPR illustrated in Figure 1 can be attributed largely to differences in the optical properties of the substrate and not to differences in nanoparticle size or shape.

The extinction spectra in Figure 1 were modeled using DDA calculations. Figure 3 shows perspective and cross-sectional

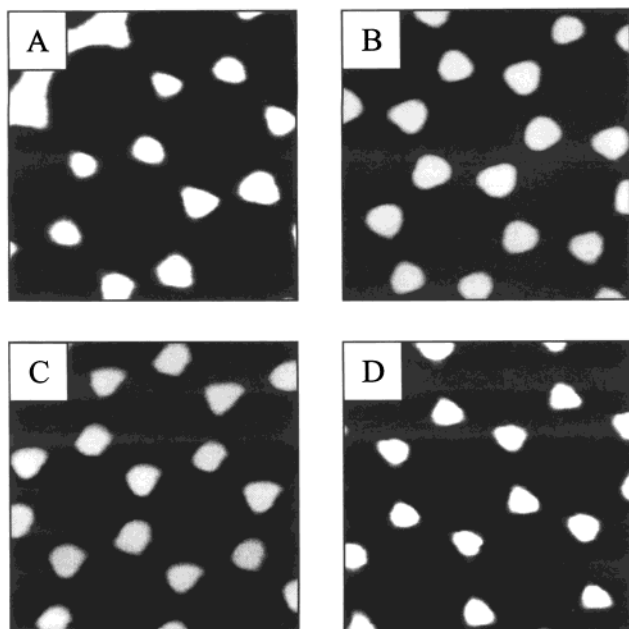


Figure 2. Tapping mode AFM images ($1.0 \mu\text{m} \times 1.0 \mu\text{m}$) of representative Ag nanoparticle arrays on various substrates. All images were collected under ambient conditions after the nanoparticles had been treated with solvent. (A) Fused silica. (B) Borosilicate optical glass. (C) Mica. (D) SF-10.

views of the arrangement of the dipoles for the nanoparticle and the substrate. The Ag nanoparticle region is a truncated tetrahedron where the perpendicular bisector (100 nm) and height (25 nm) correspond to dimensions measured by AFM. The substrate is approximated to be a finite, flat, cylindrical slab. The size of the slab is restricted by available computational resources, but we find that results generally do not change when (1) the slab thickness is larger than the particle height and (2) the slab width extends past each edge of the Ag nanoparticle by approximately the length equivalent to the nanoparticle radius. In the DDSCAT program, the physical size is denoted by the “effective radius”, the radius of a sphere of equivalent volume. Here, the effective radius of the Ag nanoparticle alone is 29.67 nm and that of the total system, Ag nanoparticle and substrate, is 60.24 nm. Figure 4 displays the calculated extinction spectra for single Ag nanoparticles on cylindrical slabs of substrate with refractive indices that match the substrates used in Figure 1. Here, λ_{max} shifts to the red from 652 nm for $n_{\text{substrate}} = 1.46$ (equivalent to fused silica) in Figure 4B to 696 nm for $n_{\text{substrate}} = 1.73$ (equivalent to SF-10) in Figure 4F. Figure 5 shows a plot of λ_{max} versus $n_{\text{substrate}}$ for both the measured and calculated extinction spectra for the Ag nanoparticles in a N_2 environment ($n_{\text{external}} = 1.0$). The slopes of the linear fits produced sensitivity factors, $\Delta\lambda_{\text{max}}/\Delta n_{\text{substrate}}$, of 87 and 155 nm RIU^{-1} for the experimental and calculated extinction spectra, respectively. This indicates that the DDA accurately predicts that the LSPR of Ag nanoparticles linearly shifts to the red with increasing $n_{\text{substrate}}$; however, the magnitude of the substrate dependence is overestimated by approximately a factor of 2 from what is observed experimentally. We have also done DDA calculations for particles that are not as oblate (3:1 ratio of perpendicular bisector to height rather than a 4:1 ratio) so that the calculated plasmon wavelength is “bluer” than in Figure 5, matching the experimental wavelength for substrates having $n_{\text{substrate}} = 1.5$. We find that the substrate sensitivity factor is similar to that for the 4:1 ratio. This shows that the difference between theory and experiment is not sensitive to uncertainties

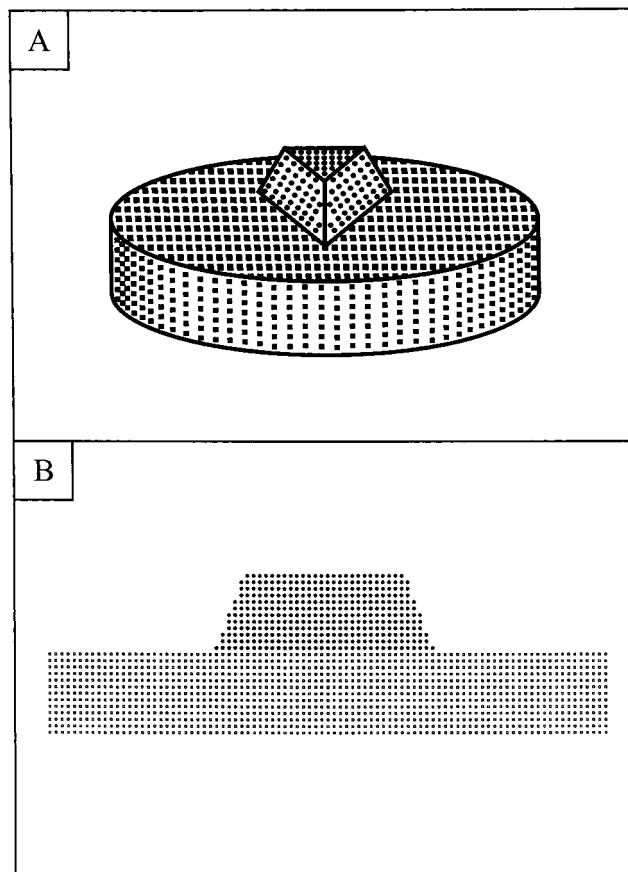


Figure 3. Schematic diagram of the DDA target. (A) Perspective view. (B) Cross-sectional view. The dipole elements are represented by circles for the Ag and squares for substrate. The Ag nanoparticle, a truncated tetrahedron with base perpendicular bisector = 100 nm and height = 25 nm, sits atop a cylindrical slab of substrate, diameter = 200 nm and height = 27 nm. These dimensions are represented by 45, 12, 90, and 13 dipole elements, respectively. The total number of dipoles used to represent the Ag nanoparticle is 11218, and the total for the nanoparticle and substrate is 93911.

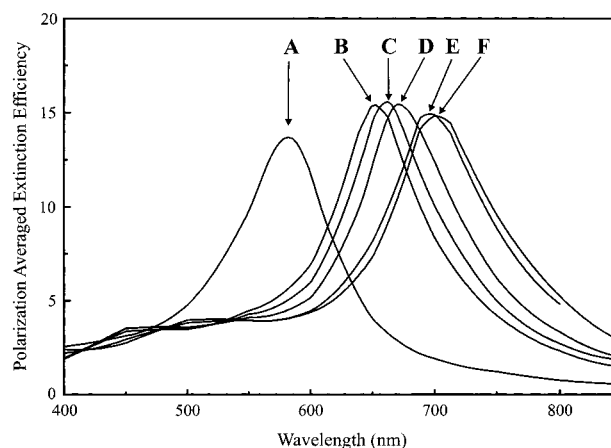


Figure 4. DDA theory results calculated using cylindrical slabs of substrate in the target geometry. The external environment was vacuum, $n_{\text{external}} = 1.0$. (A) No substrate; $\lambda_{\text{max}} = 582$ nm. (B) $n_{\text{substrate}} = 1.46$; $\lambda_{\text{max}} = 652$ nm. (C) $n_{\text{substrate}} = 1.52$; $\lambda_{\text{max}} = 661$ nm. (D) $n_{\text{substrate}} = 1.6$; $\lambda_{\text{max}} = 672$ nm. (E) $n_{\text{substrate}} = 1.73$; $\lambda_{\text{max}} = 696$ nm. (F) $n_{\text{substrate}} = 1.77$; $\lambda_{\text{max}} = 701$ nm.

in our structural model that shift the plasmon wavelength by small amounts.

A similar level of overestimation was observed previously when DDA was used to predict the influence of external solvents

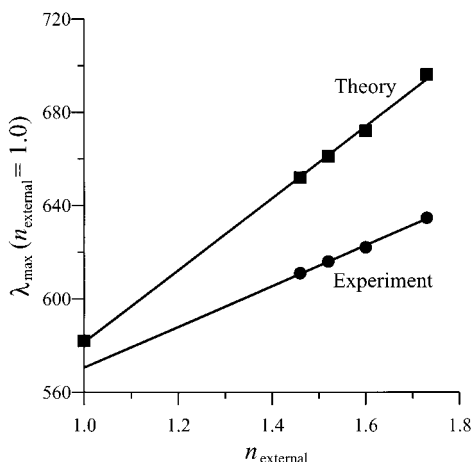


Figure 5. λ_{\max} of the LSPR of Ag nanoparticles in a N_2 environment versus the refractive index of the substrate, $n_{\text{substrate}}$. Linear regression was used to fit both data sets to lines described by the following equations: theory, $y = 155x + 426.52$; experiment, $y = 87x + 483.5$.

on the extinction spectrum of NSL-fabricated Ag nanoparticles with aspect ratio 2:1 on mica.²⁹ We will explore this comparison of theory and experiment concerning solvent and substrate effects further below.

B. Solvent Effects for Ag Nanoparticles on Various Substrates. Recently, we have begun to explore the biological and chemical sensing capabilities of NSL-fabricated Ag nanoparticles.³³ This effort, in part, has largely evolved from the study of the external dielectric dependence on the LSPR. Since NSL-fabricated nanosensors operate by measuring LSPR shifts induced by changes in the nanoparticles' local refractive index triggered by analyte binding events, it is desirable to maximize nanoparticle sensitivity to bulk environment. During initial experiments, it was observed that the extinction λ_{\max} of Ag nanoparticles on glass substrates exhibited a higher level of sensitivity to bulk external solvent than nanoparticles of the same size and shape fabricated on mica. Therefore, we hypothesized that the optical properties of the substrate may contribute to the overall LSPR sensitivity to the bulk external environment. If the substrate's contribution to bulk sensitivity is significant, it could be envisioned that judicious choice of substrate could enhance nanosensor performance. This motivation led us to measure bulk environment sensitivity factors, $\Delta\lambda_{\max}/\Delta n_{\text{external}}$, for the four different substrates used in Figure 1.

Figure 6 shows a plot of extinction peak shift, $\Delta\lambda_{\max} = \lambda_{\max}(\text{solvent}) - \lambda_{\max}(N_2)$ versus n_{external} for each of the four substrates. The slopes of the linear fits produced sensitivity factors of 238, 229, 206, and 258 nm RIU⁻¹ for fused silica, borosilicate optical glass, mica, and SF-10, respectively. From these results, we observe that the difference in sensitivity factors varies by 25% from the most sensitive substrate, SF-10, to the least sensitive substrate, mica. In terms of sensor applications, the range of 25% in sensitivity factors is encouraging. The difference in sensitivity factors when comparing SF-10 to glass is only 11%. It is likely that the slight gain in sensitivity achieved when nanoparticles are fabricated on SF-10 rather than optical glass will not offset the additional cost (\$0.25/substrate for glass, \$15/substrate for SF-10). The results presented in Figure 6 are interesting in that there appears to be no systematic correlation between the measured sensitivity factor and $n_{\text{substrate}}$. The inset of Figure 6 illustrates this observation. If the results from the SF-10 are disregarded, one could claim that the external sensitivity factor is inversely proportional to $n_{\text{substrate}}$. However, the observation that the SF-10 produces the largest sensitivity

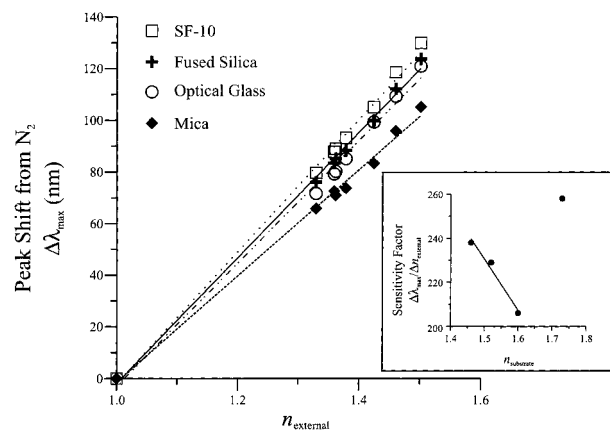


Figure 6. LSPR peak shift from N_2 , $\Delta\lambda_{\max} = \lambda_{\max}(\text{solvent}) - \lambda_{\max}(N_2)$ versus the refractive index of the solvent, n_{external} , for each of the four substrates. The plotted points represent the average shift recorded for several samples of each substrate. Each data set was fit to a line with the following equation: fused silica, $y = 238x - 241$; borosilicate optical glass, $y = 229x - 230$; mica, $y = 206x - 208$; SF-10, $y = 258x - 259$. The inset show a plot of solvent sensitivity factors (slopes) versus $n_{\text{substrate}}$. If the SF-10 point is disregarded, the sensitivity factors for the remaining three substrates can be fit to line with the equation $y = -232x + 578$.

factors was quite reproducible and was seen using Ag nanoparticles of other sizes. Thus, we believe that factors other than the bulk refractive index contribute to nanoparticle sensitivity for the SF-10 case.

DDA calculations that incorporate the substrate, Ag nanoparticle, and the surrounding external medium are computationally cumbersome. Therefore, modeling the LSPR sensitivity to bulk external medium as a function of $n_{\text{substrate}}$, as presented experimentally in Figure 6, is not practical. However, when the substrate is index-matched to the external medium ($n_{\text{substrate}} = n_{\text{external}}$), the DDA calculation becomes quite simple. Previously, we compared the sensitivity of the LSPR of NSL-fabricated Ag nanoparticles on mica (in-plane width 100 nm, out-of-plane height 25 nm) to DDA calculations generated using Ag nanoparticles with substrates and solvents that were index-matched.³¹ In this study, we disregarded the experimental contribution of the substrate and compared the sensitivities as a function of external solvent only. We found that the sensitivity factors, $\Delta\lambda_{\max}/\Delta n_{\text{external}}$, were 458 and 177 nm RIU⁻¹ for the theoretical and experimental results, respectively. Thus, theory overestimated the sensitivity to solvent by approximately a factor of 2.6. Theoretically, index matching the substrate to the external medium is feasible for any desired value of $n_{\text{substrate}}$. Unfortunately, this is not a practical experiment for the high index substrates due to chemical incompatibilities between the Ag nanoparticles and the high index fluid (viz., pyridine). However, one example of a substrate/solvent pair where $n_{\text{substrate}} = n_{\text{external}}$ is fused silica ($n = 1.46$) and carbon tetrachloride ($n = 1.46$). In addition, by using the linear fits of the data presented in Figure 6, we can extrapolate to index-matched values of λ_{\max} for each of the four substrates. Figure 7 displays a plot of λ_{\max} versus n_{medium} ($n_{\text{medium}} = n_{\text{substrate}} = n_{\text{external}}$) for both the calculated and experimental results. The experimental value of λ_{\max} for $n_{\text{medium}} = 1.0$ (no substrate in N_2 or a vacuum) is the extrapolated value from the linear fit of λ_{\max} versus $n_{\text{substrate}}$ in Figure 5. This value, 570.5 nm, was then added to the shifted amount calculated from the linear fits in Figure 6 for each of the substrates. For the index-matched results, the sensitivity factors calculated from the slopes of the linear fits for the calculated and experimental results are 487 and 239 nm RIU⁻¹, respectively. Here, the theoretical sensitivity is almost exactly

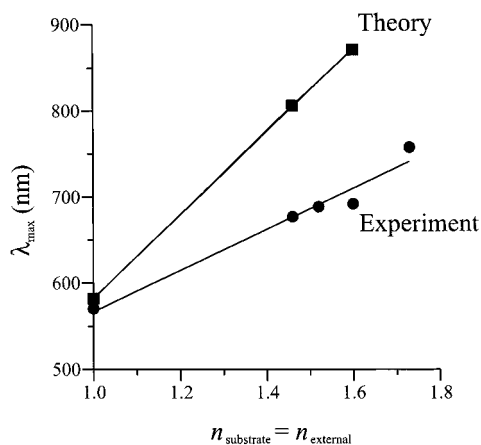


Figure 7. λ_{\max} of the LSPR versus the refractive index of the external medium for the index matched case where $n_{\text{medium}} = n_{\text{substrate}} = n_{\text{external}}$. The equation for the line through the theoretical data points is $y = 483x + 99$. The experimental data produced a line with equation $y = 239x + 328$.

twice of that observed experimentally. This is a bit of an improvement when compared to the factor of 2.6 previously seen when the experimental results disregarded the substrate contribution.

Using the results presented in this paper, one can compare the solvent and the substrate contributions to the sensitivity of the LSPR. Experimentally, it is impossible to observe the solvent only component since a successful method for removing the Ag nanoparticles from the substrate intact has yet to be developed. However, if one assumes that the substrate and solvent sensitivity components add to produce the overall sensitivity to bulk environment, the solvent sensitivity can be computed when the overall and substrate sensitivities are known. From Figure 7, the overall experimental sensitivity was 239 nm RIU^{-1} . By subtracting the substrate sensitivity of 87 nm RIU^{-1} generated from the data in Figure 5, the solvent sensitivity is calculated to be 152 nm RIU^{-1} . Likewise for the theoretical results, the derived solvent sensitivity is 328 nm RIU^{-1} (483 nm RIU^{-1} (solvent plus substrate) $- 155 \text{ nm RIU}^{-1}$ (substrate)). Consequently, the solvent:substrate ratios for the sensitivity factors are 1.75 and 2.12 for the experimental and DDA results, respectively. This demonstrates that theory and experiment agree on the ratios of sensitivities, even though the sensitivities themselves differ by a factor of 2.

Intuitively, it makes sense that the Ag nanoparticles have higher sensitivities to bulk solvent because a larger fraction of the surface area is exposed to solvent than to the substrate. Using the approximated three-dimensional shape of a truncated tetrahedron, simple geometry can be used to calculate the amount of surface area of the Ag nanoparticle exposed to both the solvent and substrate. For a nanoparticle with a perpendicular bisector of 100 nm and height of 25 nm, the surface area exposed to solvent (the three truncated sides plus the top face) is approximated to be $11\,063 \text{ nm}^2$, while the surface exposed to the substrate is 5774 nm^2 . Therefore, the solvent:substrate exposed surface area ratio is 1.9:1, nearly 2:1. Comparing the ratio of sensitivity factors to the ratio of surface areas, we find experimentally that the sensitivity ratio is about 9% less than what the geometric ratios predicted. Conversely, the theoretical sensitivity ratio is approximately 11% higher. From these findings, we can conclude that our assumption that the overall sensitivity factor is the sum of the individual solvent and substrate sensitivities is correct within experimental error. Furthermore, the discrepancies between the geometrical ratios

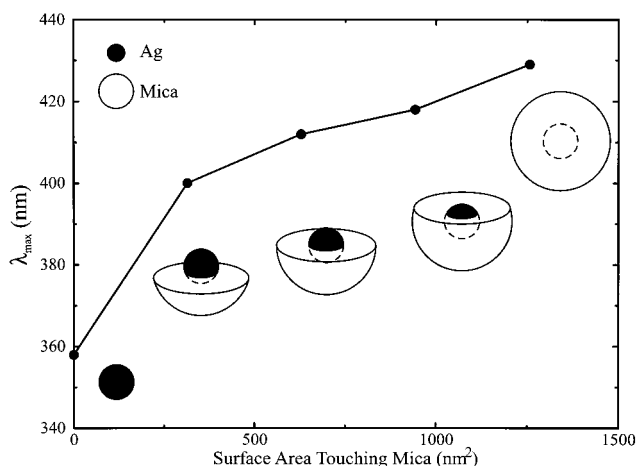


Figure 8. DDA results showing LSPR wavelength as a function of particle area in contact with substrate. The DDA calculations are for a Ag core of radius 10 nm and a partial mica shell of radius 30 nm. Degree of embedding is changed by truncating the mica shell at $z = -5, 0,$ and 5 nm , along an axis where the origin is the center of the sphere, as depicted.

and the sensitivity ratios can be attributed to deviations in the true nanoparticle shape from the idealized shape of the truncated tetrahedron.

To probe the idea that the LSPR shift varies with the area in contact with the substrate, we have done additional DDA calculations that model a silver sphere sinking into a substrate. Figure 8 shows the results for a 10 nm sphere engulfed by a mica substrate, including the cases where no mica is present (i.e., sphere surrounded by vacuum) and when the Ag core is completely enclosed. We see that the LSPR wavelength shifts dramatically to the red as the sphere goes from free to being partially embedded (25% of the sphere area is exposed to mica). As the sphere becomes increasingly more embedded (area exposed to mica varies from 25% to 100%), the shift to the red is much slower, and is approximately linear with exposed area. This shows that our “exposed area” hypothesis does work, but only for a limited range of parameters. Effective medium theories have also been proposed to explain the spectra of partially embedded objects;¹ however, the relative volumes of the two media have not been defined, except for the simple case of a half-embedded object. Most likely, the exposed area and effective medium ideas are deficient because they fail to account for the change in LSPR wavelength that arises from the asymmetric environment that the particle experiences. Indeed, the exposed area and effective medium approaches do not distinguish between single layers or multiple layers, and they do not describe such features as the asymmetry in the interaction of the induced dipole with its image in the surrounding medium.

IV. Conclusions

The results presented in this paper demonstrate that the optical properties of surface-confined nanoparticles fabricated via NSL depend on the substrate on which they have been fabricated. For Ag nanoparticles with an aspect ratio of 4:1 in a controlled N_2 environment, the LSPR peak λ_{\max} shifts to the red as the refractive index of the substrate is increased. The relationship between λ_{\max} and $n_{\text{substrate}}$ is approximately linear with a sensitivity factor, $\Delta\lambda_{\max}/\Delta n_{\text{substrate}}$, of 87 nm RIU^{-1} . DDA theory was used to calculate extinction spectra of Ag nanoparticles on substrate slabs using refractive indices that matched the substrates used experimentally. The DDA results qualitatively

predicted that λ_{\max} shifts to the red with increasing $n_{\text{substrate}}$; however, the calculated sensitivity factor was almost twice that measured experimentally. There are two possible reasons for this large disparity between theory and experiment. In a previous investigation, we showed that the LSPR of Ag nanoparticles is extremely sensitive to nanoparticle size and shape.³² Therefore, small deviations in the true nanoparticle shape from the theoretical approximation of the truncated tetrahedron is one reason for the quantitative disagreement between the DDA calculations and experimental results for the nanoparticle in a controlled N₂ environment. Work is currently underway to refine the theoretical nanoparticle shape to include structural rearrangement and edge-annealing effects observed when the nanoparticles are exposed to solvent.³³ A second reason concerns the dielectric function at the metal/surface or metal/solvent interface. Previously, we found that the theoretical model overpredicts solvent effects, suggesting that the solvent is not directly in contact with the nanoparticle. Indeed, it is known that oxide layers on noble metal surfaces can significantly perturb the metal dielectric response.³⁹ In addition, the metal may interact chemically with the substrate and/or the solvent, thereby changing the effective dielectric response near the interface.

Additionally, we demonstrated that the sensitivity of Ag nanoparticles to bulk external environment also varies with substrate. However, it is difficult to conclude that the sensitivity is dependent upon $n_{\text{substrate}}$ since the SF-10 and mica substrates (the two largest values of $n_{\text{substrate}}$ 1.73 and 1.6) produced the highest and the lowest sensitivities, respectively. If the value of SF-10 is disregarded, it could be substantiated that the measured sensitivity is inversely proportional to $n_{\text{substrate}}$. Since the SF-10 result is quite reproducible, it is difficult to consider it anomalous. Consequently, we believe that factors other than the refractive index are at least partially contributing to the enhanced sensitivity seen with SF-10. One possibility for this observation could be that Ag atoms in the nanoparticle bind to lead dopant atoms in the SF-10. The Ag–Pb bonds alter the surface electronic structure of the nanoparticle, which in turn affects the sensitivity to bulk environment. Another possibility is that the dopant ions leach out from the substrate and bind to the nanoparticle, modifying the thin oxide contamination layer mentioned above. Since the theoretical results indicate much larger solvent shifts than seen in the experiment, any change in the oxide layer (or in the nature of the chemical interaction between the solvent and nanoparticle) could have major consequences.

DDA calculations were performed for Ag nanoparticles on substrates index matched to the external medium. This condition is significantly easier to model theoretically than when $n_{\text{substrate}}$ is different from n_{external} . When compared to the experimental index-matched results extrapolated from the data in Figure 6, theory again overestimates the sensitivity by approximately a factor of 2. This level of overestimation is consistent with what was observed for the substrate sensitivity in Figure 5. By subtracting the substrate sensitivity from the index-matched sensitivity, we calculated the solvent sensitivities to be 152 and 332 nm RIU⁻¹ for the experimental and theoretical results, respectively. When compared to substrate sensitivities, the solvent sensitivity is 1.75 times larger, experimentally, and 2.10 times larger, theoretically. These factors are intuitive when considering the ratio of nanoparticle surface area exposed to solvent versus that exposed to substrate. Both the experimental and theoretical ratios of solvent:substrate sensitivity factors are within $\pm 10\%$ of the calculated ratio of solvent:substrate exposed

nanoparticle surface areas. Again, these discrepancies can be attributed to deviations in the true nanoparticle shape from the approximated truncated tetrahedron. However, the idea that plasmon shift is proportional to exposed area is oversimplified, as demonstrated in our studies of an engulfed sphere. Despite significant discrepancies in absolute values of sensitivity factors, we conclude that the DDA is a useful tool to predict the LSPR sensitivity to nanoparticle environment.

Acknowledgment. This research was supported by the ARO (Grant DAAG55-97-1-0133), NSF (Grant CHE-940078), and the MRSEC program of the NSF (Grant DMR-9632472). We also thank Professor Joseph T. Hupp for access to the Digital Instruments Bioscope.

References and Notes

- (1) Kreibig, U.; Vollmer, M. *Optical Properties of Metal Clusters*; Springer-Verlag: Heidelberg, Germany, 1995; Vol. 25.
- (2) Champion, A.; Kambhampati, P. *Chem. Soc. Rev.* **1998**, *27*, 241–250.
- (3) Hilger, A.; Cüppers, N.; Tenfelde, M.; Kreibig, U. *Eur. Phys. J. D* **2000**, *10*, 115–118.
- (4) Dirix, Y.; Bastiaansen, C.; Caseri, W.; Smith, P. *Adv. Mater.* **1999**, *11*, 223–227.
- (5) Kroschwitz, J. I.; Howe-Grant, M. Glass. In *Encyclopedia of Chemical Technology*, 4th ed.; Kroschwitz, J. I., Howe-Grant, M., Eds.; John Wiley & Sons: New York, 1994; Vol. 12, pp 569–571.
- (6) Quinten, M.; Leitner, A.; Krenn, J. R.; Aussenegg, F. R. *Opt. Lett.* **1998**, *23*, 1331–1333.
- (7) Krenn, J. R.; Dereux, A.; Weeber, J. C.; Bourillot, E.; Lacroute, Y.; Goudonnet, J. P. *Phys. Rev. Lett.* **1999**, *82*, 2590–2593.
- (8) Ebbesen, T. W.; Lezec, H. J.; Ghaemi, H. F.; Thio, T.; Wolff, P. A. *Nature* **1998**, *391*, 667–669.
- (9) Pendry, J. B. *Science* **1999**, *285*, 1687–1688.
- (10) Sánchez, E. J.; Novotny, L.; Xie, X. S. *Phys. Rev. Lett.* **1999**, *82*, 4014–4017.
- (11) Knoll, B.; Kellmann, F. *Nature* **1999**, *399*, 134–137.
- (12) Hamann, H. F.; Gallagher, A.; Nesbitt, D. J. *Appl. Phys. Lett.* **1998**, *73*, 1469–1471.
- (13) Novotny, L.; Bian, R. X.; Xie, S. *Phys. Rev. Lett.* **1997**, *79*, 645–648.
- (14) Pufall, M. R.; Berger, A.; Schultz, S. J. *Appl. Phys.* **1997**, *81*, 5689–5691.
- (15) Jensen, T. R.; Van Duyne, R. P.; Johnson, S. A.; Maroni, V. A. *Appl. Spectrosc.* **2000**, *54*, 371–377.
- (16) Wadayama, T.; Suzuki, O.; Takeuchi, K.; Seki, H.; Tanabe, T.; Suzuki, Y.; Hata, A. *Appl. Phys. A* **1999**, *69*, 77–80.
- (17) Tarcha, P. J.; DeSaja-Gonzalez, J.; Rodriguez-Llorente, S.; Aroca, R. *Appl. Spectrosc.* **1999**, *53*, 43–48.
- (18) Emory, S. R.; Nie, S. J. *Phys. Chem. B* **1998**, *102*, 493–497.
- (19) Nie, S.; Emory, S. R. *Science* **1997**, *275*, 1102–1106.
- (20) Yang, W. H.; Hulteen, J. C.; Schatz, G. C.; Van Duyne, R. P. *J. Chem. Phys.* **1996**, *104*, 4313–4323.
- (21) Freeman, R. G.; Grabar, K. C.; Allison, K. J.; Bright, R. M.; Davis, J. A.; Guthrie, A. P.; Hommer, M. B.; Jackson, M. A.; Smith, P. C.; Walter, D. G.; Natan, M. J. *Science* **1995**, *267*, 1629–1632.
- (22) Pipino, A. C. R.; Schatz, G. C.; Van Duyne, R. P. *Phys. Rev. B* **1996**, *53*, 4162–4169.
- (23) Van Duyne, R. P.; Hulteen, J. C.; Treichel, D. A. *J. Chem. Phys.* **1993**, *99*, 2101–2115.
- (24) Bauer, G.; Pittner, F.; Schalkhammer, T. *Mikrochim. Acta* **1999**, *131*, 107–114.
- (25) Storhoff, J. J.; Elghanian, R.; Mucic, R. C.; Mirkin, C. A.; Letsinger, R. L. *J. Am. Chem. Soc.* **1998**, *120*, 1959–1964.
- (26) Elghanian, R.; Storhoff, J. J.; Mucic, R. C.; Letsinger, R. L.; Mirkin, C. A. *Science* **1997**, *277*, 1078–1081.
- (27) Kreibig, U.; Gartz, M.; Hilger, A. *Ber. Bunsen-Ges. Phys. Chem.* **1997**, *101*, 1593–1604.
- (28) Hulteen, J. C.; Van Duyne, R. P. *J. Vac. Sci. Technol., A* **1995**, *13*, 1553–1558.
- (29) Hulteen, J. C.; Treichel, D. A.; Smith, M. T.; Duval, M. L.; Jensen, T. R.; Van Duyne, R. P. *J. Phys. Chem. B* **1999**, *103*, 3854–3863.
- (30) Jensen, T. R.; Schatz, G. C.; Van Duyne, R. P. *J. Phys. Chem. B* **1999**, *103*, 2394–2401.
- (31) Jensen, T. R.; Duval, M. L.; Kelly, L.; Lazarides, A.; Schatz, G. C.; Van Duyne, R. P. *J. Phys. Chem. B* **1999**, *103*, 9846–9853.

- (32) Jensen, T. R.; Duval Malinsky, M.; Haynes, C. L.; Van Duyne, R. P. *J. Phys. Chem. B* **2000**, *104*, 10549–10556.
- (33) Duval Malinsky, M.; Kelly, L.; Schatz, G. C.; Van Duyne, R. P. *J. Am. Chem. Soc.* **2001**, in press.
- (34) Jensen, T. R.; Kelly, L.; Lazarides, A.; Schatz, G. C. *J. Clust. Sci.* **1999**, *10*, 295–317.
- (35) Draine, B. T.; Flatau, P. J. *J. Opt. Soc. Am. A* **1994**, *11*, 1491.
- (36) Yang, W. H.; Schatz, G. C.; Van Duyne, R. P. *J. Chem. Phys.* **1995**, *103*, 869–875.
- (37) Draine, B. T.; Flatau, P. J. *Program DDSCAT*; University of California, San Diego, Scripps Institute of Oceanography, 8605 La Jolla Dr., La Jolla, CA 92093-0221.
- (38) Palik, E. D. *Handbook of Optical Constants of Solids*; Academic Press, Inc.: New York, 1985.
- (39) Wismann, P. Optical Properties of Thin Metal Films Interacting with Gases. In *Handbook of Optical Properties. Optics of Small Particles, Interfaces, and Surfaces*; Hummel, R. E. W. P., Ed.; CRC Press: Boca Raton, FL, 1997; Vol. II, pp 401–446.